Colloid Polym Sci (2005) 283: 1321–1333
DOI 10.1007/s00396-005-1346-x

ORIGINAL CONTRIBUTION

Julius Tsuwi
Dietmar Appelhans
Stefan Zschoche
Rong-Chuan Zhuang
Peter Friedel
Liane Häußler
Brigitte Voit
Friedrich Kremer

Molecular dynamics in fluorinated side-chain maleimide copolymers as studied by broadband dielectric spectroscopy

Received: 27 October 2004
Accepted: 14 April 2005
Published online: 5 July 2005

J. Tsuwi (✉) · F. Kremer
Institute for Experimental Physics I,
University of Leipzig, Linné Strasse 5,
04103 Leipzig, Germany

D. Appelhans · S. Zschoche
R.-C. Zhuang · P. Friedel
L. Häußler · B. Voit
Leibniz Institute of Polymer Research
Dresden, Hohe Strasse 6,
01069 Dresden, Germany

Abstract A series of alternating maleimide (MI) copolymers with fluorinated side chains have been investigated using broadband dielectric spectroscopy. The side chains consist of fluoroalkane ($-C_xF_{2x+1}$, $x = 1, 7, 9$) end groups connected to the main chain via methylene spacers. The experiments were carried out in a frequency range of 0.1 Hz to 10 MHz and at temperatures between 120 K and 500 K. The fluorinated MI copolymers show a fast sub-T_g (β) relaxation characterized by an Arrhenius-type temperature dependence with activation energy in the range of 30–37 kJ/mol. Two more processes (α and δ-like) are observed, corresponding to independent relaxations of the main chain and the fluoroalkane domains respectively. For shorter side chains, the δ-like process is not observed but instead another relaxation process, α_S, occurs at temperatures higher than either the α and δ-like processes. When compared with unfluorinated MI copolymers, the fluorinated MI copolymers show the δ-like process and a slower β-relaxation unlike their unfluorinated counterparts. A model to explain the molecular origin of the four processes is proposed, supplemented by differential scanning calorimetry and published WAXS/SAXS data.

Keywords Dielectric spectroscopy · Molecular dynamics · Microphase separated · Fluoropolymers · Maleimide copolymer

Introduction

Materials consisting of perfluoroalkyl groups offer a wide range of interesting properties, such as wettability, durability, and thermal stability [1, 2]. The hydrophobic nature (i.e. very low solid surface tension) of fluoropolymers is utilized for the development of coatings with low wetting behavior. Such modified surfaces can be used, for example, as soil release agents on different substrates such as textiles [3], paper [4], leather carpets [5] and also to prevent the attachment of microorganisms such as algae and other marine life. Although wettability (water/oil repellency) is confined to the surface, the need to have mechanically stable materials in the bulk coupled with the excellent surface properties is vital. It is well known that microphase separation occurs in structural segments consisting of alkyl and perfluoroalkyl groups [6–8] resulting in highly ordered layers with the $-CF_3$ groups at the surface. Thus, perfluorinated molecules have been incorporated in polymer backbones [9, 10] and as side chains [7, 11–17] in order to study the optical, thermal, dielectric and surface properties both in the bulk [7, 10–13, 18] and as thin films [19–21]. Acrylic [9], methacrylic [9] and styrenic [10] backbones have been used with varying lengths of alkyl and

perfluoroalkyl units on the side chain to investigate liquid crystalline behavior. Other studies involving carbosilane dendrimers [14–16], polyesters [7] and block copolymers [18, 22, 23] as backbones with fluorinated side chains have also been carried out.

Although the effect of fluorination on surface and bulk properties has been investigated, few studies [19, 20, 24] have used maleimides (MI) as the polymer backbone. The simple synthetic approach of MI copolymers by polymer analogous reaction of maleic anhydride copolymers (Scheme 1) allows the introduction of different kinds of side chains to achieve either hydrophilic [25] or hydrophobic [26] properties. MI copolymers with modified side chains therefore find their use in surface engineering applications. Practically nothing is known about the molecular dynamics in fluorinated MI copolymers. In this paper, dielectric spectroscopy is employed to study the dynamics of MI copolymers with *N*-(2,2,2-trifluoro)ethyl, *N*-(4-(*N*-perfluoroheptylcarbonyl)aminobutyl, *N*-(4-(*N*-perfluorononylcarbonyl)aminobutyl and *N*-(6-(*N*-perfluorononylcarbonyl)aminohexyl side chains. The fluorinated side chains (Scheme 1, R^1) consist of perfluoroalkyl segments attached to the maleimide ring via CH_2 spacer unit(s). Three different MI copolymer main chains are used namely, poly(ethene-*alt*-maleimide) (ETM), poly(styrene-*alt*-maleimide) (STM) and poly(octadecene-*alt*-maleimide) (ODM). Except for ETM, the backbones of STM and ODM possess a second side group R^2 on the main chain (Scheme 1). Recently [27, 28], we used dielectric spectroscopy to investigate the dynamics of MI copolymers with *n*-alkyl side chains. The molecular motion of the MI backbone was described. In the present work, information on the dynamics of the perfluoroalkyl-containing side chains (which are dielectrically active) under different main chain structures is reported. The effect of varying the length of the perfluoroalkyl chain and the alkyl spacer units on the molecular dynamics will be analyzed. Finally, we will compare the dynamics of the perfluorinated side chains (to be referred in the paper as R_f) with unfluorinated (R_h) (only with methylene groups) ones of similar lengths. The interpretation of the results will be supported by differential scanning calorimetry (DSC) and published wide- and small-angle X-ray (WAXS/SAXS) data.

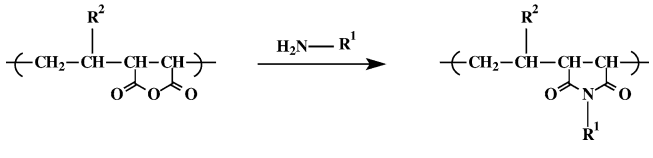

Scheme 1 Reaction of maleic anhydride (MA) to form MI copolymers

Experimental

Synthesis and characterization of fluorinated (R_f) monomers and copolymers

Chemicals

Alternating maleic anhydride copolymers poly(ethene-*alt*-maleic anhydride) (M_w 125,000 g/mol) (Aldrich, Munich, Germany), 2,2,2-trifluoroethylamine and methyl perfluorodecanoate (ABCR GmbH & Co. KG, Karlsruhe, Germany), 1,4-diaminobutane and 1,6-diaminohexane (ACROS Organics, Geel, Belgium) were purchased and used as received.

Details of the synthesis and characterization of monomer *N*-(4-aminobutyl)perfluorooctaneamide hydro chloride and MI copolymers ETM4F15, STM4F15, ODM4F15, ETMH25, STMH25, and ODMH25 are found elsewhere [24]. In this section, we describe the synthesis of *N*-(4-aminobutyl)perfluorodecaneamide hydro chloride and *N*-(6-aminohexyl)perfluorodecaneamide hydro chloride monomers and MI copolymers ETM1F3, ETM4F19, and ETM6F19.

N-(4-aminobutyl)perfluorodecaneamide hydro chloride

1,4-Diaminobutane (0.349 g; 3 mmol) was dissolved in 15 ml of anhydrous methanol under nitrogen atmosphere. Methyl perfluorodecanoate (1.056 g; 2 mmol) was slowly added to the reaction solution at room temperature and the reaction mixture was stirred at room temperature for 1 h and then at 40 °C for 20 h. During the reaction, phase separation occurred between the fluorinated monomer and the organic solution. The solvent was distilled off under vacuum and the residual was suspended in diethyl ether and acidified with very diluted aqueous hydrogen chloride solution. The resulting solid was washed with diethyl ether and water sequentially and then dried in a vacuum oven at 40 °C for 2 days to yield 1.115 g (89.8%) of *N*-(4-aminobutyl)perfluorodecaneamide hydro chloride as white solid. The characterization results can be summarized as follows: melting point 207–212 °C. ^{1}H NMR (DMSO-d_6:$CDCl_3$ = 1:1): $\delta = 1.57$ (m, 2H, $R_fCONHCH_2CH_2$); 1.58 (m, 2H, $CH_2CH_2NH_2{\cdot}HCl$); 2.78 (m, 2H, $CH_2NH_2{\cdot}HCl$); 3.22 (q, 2H, $R_fCONHCH_2$); 7.91 (s, 3H, $CH_2NH_2{\cdot}HCl$); 9.31 ppm (t, 1H, R_fCONH). ^{13}C NMR (DMSO-d_6:$CDCl_3$ = 1:1): $\delta = 24.08$ ($CH_2CH_2NH_2{\cdot}$ HCl); 25.21 ($R_fCONHCH_2CH_2$); 38.43 ($CH_2NH_2{\cdot}HCl$); 38.65 ($R_fCONH\ CH_2$); 156.74 ppm (R_fCONH). ^{19}F NMR (DMSO-d_6:$CDCl_3$ = 1:1): $\delta = -81.29$ (CF_3), −119.62 (CF_2–CO), −122.42, −123.11, −123.33 and −126.69 ppm (CF_2).

N-(6-aminohexyl)perfluorodecaneamide hydro chloride

1,6-Diaminohexane (0.174 g; 1.5 mmol) was dissolved in 8 ml of anhydrous methanol under nitrogen atmosphere. Methyl perfluorodecanoate (0.528 g; 1 mmol) was slowly added to the reaction solution at room temperature. The rest of the procedure is the same as the one described for the R_f-monomer *N*-(4-aminobutyl)perfluorodecaneamide hydro chloride. At the end of the synthesis, a white solid 0.585 g (90.2%) of *N*-(6-aminohexyl)perfluorodecaneamide hydro chloride was obtained. The resultant material characteristics are as follows: melting point 188–191°C. ^{1}H NMR (DMSO-d_6:$CDCl_3$ = 1:1): δ = 1.28 (m, 2H, $R_fCONHCH_2CH_2CH_2$); 1.32 (m, 2H, $CH_2CH_2CH_2NH_2{\cdot}HCl$); 1.49 (m, 2H, $R_fCONHCH_2CH_2$); 1.57 (m, 2H, $CH_2CH_2NH_2{\cdot}HCl$); 2.74 (m, 2H, $CH_2NH_2{\cdot}HCl$); 3.19 (q, 2H, $R_fCONHCH_2$); 7.88 (s, 3H, $CH_2N\,H_2{\cdot}HCl$); 9.20 ppm (t, 1H, R_fCONH). ^{13}C NMR (DMSO-d_6:$CDCl_3$ = 1:1): δ = 25.31 ($CH_2CH_2CH_2NH_2{\cdot}HCl$); 25.45 ($R_fCONHCH_2CH_2CH_2$); 26.77 ($CH_2CH_2NH_2{\cdot}HCl$); 27.89 ($R_fCONHCH_2\ CH_2$); 38.83 ($CH_2NH_2{\cdot}HCl$); 39.12 ($R_fCONH\ CH_2$); 156.62 ppm ($R_fCONH$). ^{19}F NMR (DMSO-$d_6$:$CDCl_3$ = 1:1): δ = −81.29 (CF_3), −119.62 (CF_2-CO), −122.42, −123.11, −123.33 and −126.69 ppm (CF_2).

Copolymers ETM1F3, ETM4F19 and ETM6F19

A volume of 1.0 mol of poly(ethene-*alt*-maleic anhydride), 1.0 mol of triethylamine and 1.0 mol of amino compound (2,2,2-trifluoroethylamine, *N*-(4-aminobutyl)perfluorodecaneamide hydro chloride or *N*-(6-aminohexyl)perfluoro-decaneamide hydro chloride) were dissolved in tetrahydrofurane and stirred at 160 °C for 24 h in an autoclave. The cooled reaction solution was poured into acidic water solution. The resulting MI copolymers were washed intensively with water and then dried in vacuum at 40 °C. Characterization of the copolymers with IR spectroscopy showed a complete conversion of the maleic anhydride ring into the maleimide ring. Fluorine elemental analyses were done for the MI copolymers with longer perfluoroalkyl segments in order to calculate the degree of attached R_f-side chains (Table 1).

The fluorine analyses were carried out by the Beller Microanalytic Laboratory (Göttingen, Germany). The nuclear magnetic resonance (NMR) measurements performed on the monomers were done in 5 mm o.d. sample tubes with a BRUCKER DRX 500 NMR spectrometer operating at 500.13 MHz for ^{1}H, at 470.59 MHz for ^{19}F, and at 125.75 MHz for ^{13}C. DMSO-d_6 and $CDCl_3$ in 1:1 ratio were used as solvent for all the NMR experiments. For internal calibration the solvent peaks of DMSO-d_6 were used: δ (^{13}C) = 39.60 ppm; δ (^{1}H) = 2.50 ppm. The ^{19}F NMR spectra were referenced to internal C_6F_6 (δ (^{19}F) = −163 ppm). The signal assignment was done by ^{1}H–^{1}H COSY and ^{1}H–^{13} C HMQC 2D NMR measurements using the standard pulse sequences provided by BRUCKER.

Bulk properties of fluorinated MI copolymers ETM4F15, STM4F15 and ODM4F15, and unfluorinated MI copolymers ETMH25, STMH25 and ODMH25

In order to describe the molecular dynamics of MI copolymers fully, it was necessary to understand the

Table 1 Average degree of repeating unit (RU) for alkene-maleic anhydride (AM) used in poly(alkene-*alt*-maleic anhydride)s, molecular mass (M) of the RU in MI copolymer, the found/calculated data for fluorine (F), calculated degree of attached side chains in MI and calculated molecular weights of MI

MI copolymer	∅ Degree of RU AM[a]	M of RU[b] (g/mol)	F[c] (wt%)	F[d] (wt%)	Degree of side chains	M_w^e (×10^3 g/mol)
ETM1F3	992	207.15	27.51	–[g]	˜0.95–1[h]	˜200
ETM4F15[f]	992	592.30	48.11	44.01	0.91[i]	˜548
ETMH25[f]	992	293.44	–	–	0.95–1[h]	˜291
ETM4F19	992	692.32	52.14	50.49	0.97[i]	˜666
ETM6F19	992	720.37	50.11	47.86	0.95[i]	˜678
STM4F15[f]	99	668.40	42.64	40.50	0.95[i]	˜63
STMH25[f]	99	369.54	–	–	0.95–1[h]	˜36
ODM4F15[f]	86–143	816.73	34.89	33.37	0.96[i]	˜67–112
ODMH25[f]	86–143	517.87	–	–	0.95–1[g]	˜44–74

[a]Molecular weight of converted poly(ethene-*alt*-maleic anhydride) 125,000 g/mol (Aldrich, Germany), of converted poly(styrene-*alt*-maleic anhydride) 20,000 g/mol (Leuna Werke AG, Germany), and of poly(octadecene-*alt*-maleic anhydride) 30,000–50,000 g/mol (Polyscience Inc., USA)
[b]Molecular mass (M) of repeating unit (RU) with R^1 and R^2 in MI copolymers (Scheme 1)
[c]Theoretical data
[d]Values obtained from fluorine analysis
[e]Calculated data based on ∅ degree of RU AM including values from h and i
[f]Presented in ref. [24]
[g]Not determined
[h]Based on ATR-IR results
[i]Based on found F content

bulk properties of the materials. Therefore, glass transition (T_g) and melting (T_m) temperatures were determined on a DSC Q1000 (TA Instrument) over a temperature interval of 193–473 K at a scan rate of ±20 K/min. The T_g's were determined using the half step method from the second heating runs. The results of WAXS (ETM4F15, STM4F15, ODM4F15, ETMH25, STMH25, and ODMH25), SAXS (ETMF4F15 and ODM4F15) and DSC thermogram of ETMF15 are discussed in detail elsewhere [24]. Additionally, temperature-dependent ATR-IR investigations on ETM4F15, STM4F15 and ODM4F15 (to prove H-bonding interactions within the perfluorinated amide groups from room temperature to T_m and also above T_m), and temperature-dependent SAXS results on ETM4F15 (to reveal reversible and defined layered structures) can also be found in ref. [24]. For the purpose of this paper, only a summary is presented in Table 2 and a brief discussion of DSC for selected samples will be made. The MI copolymers also exhibit backbone-to-backbone distances, *d*, in the range 2.48–3.42 nm [24]. For ETM4F15 a thermally stable layer was observed over a wide temperature range. Exception is found in sample ODM4F15, which shows a broad SAXS signal interpreted as no defined layer structure. In general, and with the support of WAXS, SAXS, DSC and ATR-IR investigations, layered structures are assumed at room temperature where partly ordered side chain organizations are present, which are influenced by the alternating substitution pattern of the main chains and the H-bonding interactions in fluorinated MI copolymers. Such layered structures are presumed to exist above T_m's for ETM4F19, ETM6F19 and ETMH25 from investigations done on ETM4F15. All the materials under study are amorphous as reported in ref. [24].

Molecular modeling

The molecular modeling calculations were carried out on a LINUX operating system, SuSE Distribution 8.2 [29] Kernel 2.4. The geometry and the conformation of the monomer units were optimized by means of quantum mechanical ab initio calculations using GAMESS [30, 31] software by applying a 6-31G** (with diffuse orbitals: for H as $+2p$ and for C, N, O, and F as $+3s$ and $+3p$) basis set of the restricted and unrestricted Hartree-Fock self consistent field approach, additionally for charge evaluation on parts of the polymer molecules (CH_3–CH_2-radical, CF_3-CF_2-radical, longer alkyl and perfluoroalkyl segments, CF_4 and CH_4, *N*-methyl-succinimide, Ethylbenzene as monomer like units). Dipole moment calculations were done using all coordinates of atoms of the part structure and monomer conformation and the relative atomic charges obtained from the quantum mechanical ab initio calculations.

Dielectric measurements and data analysis

To prepare the samples, MI materials were heated in vacuum until they melted and kept between two brass electrodes (diameter: 10 mm) with 50 µm glass fiber spacers. Isothermal dielectric measurements were performed in the frequency range from 0.1 Hz to 10 MHz using a high resolution dielectric alpha-analyzer (Novocontrol GmbH). Dielectric spectra were obtained starting from the highest temperature for the range 120–500 K in steps of 2 K. The sample temperature was controlled by a gas heating system based on the evaporation of liquid nitrogen (Quatro, Novocontrol GmbH) with a precision of ±0.02 K. Details of the set up are found in ref. [32].

Table 2 Thermal properties of poly(alkene-*alt*-*N*-$R_{f,h}$-alkylmaleimide) copolymers, obtained from DSC (at rate 20 K/min), used in the study

MI copolymer	Second heating run			Cooling after first heating	
	T_g (K)	T_m (K)	Δ H_m (J/g)	$T_{c,m}$ (K)	ΔH_c (J/g)
ETM1F3	392.2	–	–	–	–
ETM4F15[a]	373.2	436.2	3.3	425.2/430.2	−3.2
ETMH25[a]	330.2	235.2	11.8	–[b]	–[b]
ETM4F19	–	433.6	17.0	422.0	−10.2
		465.0	0.5	456.7	–0.8
ETM6F19	299.4	396.8	7.2	383.0	−5.5
		402.2			
		416.5			
		449.9	1.2	438.5	−1.3
STM4F15[a]	386.2	–	–	–	–
STMH25[a]	343.2	–	–	–	–
ODM4F15[a]	336.2	251.2	1.9	–[b]	–[b]
ODMH25[a]	303.2	251.2	20.9	–[b]	–[b]

[a]Published in ref. [24]
[b]Not calculated because of program temperature deviates from sample temperature below 253 K

For quantitative analysis, the dielectric loss ε″ was fitted to a superposition of a conductivity contribution with one or two relaxation functions according to Havriliak and Negami [33].

$$\varepsilon''(\omega) = \frac{\sigma_o}{\varepsilon_o}\frac{a}{\omega^s} + \mathrm{Im}\left[\frac{\Delta\varepsilon}{\left[1+(i\omega\tau)^{\beta}\right]^{\gamma}}\right] \quad (1)$$

The first part on the right hand side of the equation describes the conductivity while the second part (that is added) is the imaginary part of the dielectric function. In this notation, one relaxation process is assumed. β and γ are dimensionless parameters describing the symmetric and asymmetric broadening of the distribution of relaxation times respectively with $0 < (\beta,\beta\gamma) \leq 1$. For $\beta = \gamma = 1$, Eq. 1 coincides with the ideal Debye-relaxation. ε_o is the permittivity of free space and σ_o is the direct current (d.c) conductivity. The exponent s equals one for Ohmic behavior, deviations ($s < 1$) are caused by electrode polarization or Maxwell–Wagner polarization effects, and a is a factor having the dimensions $[\mathrm{Hz}]^{s-1}$ for $s \neq 1$. From the fits according to Eq. 1 the relaxation rate $1/\tau_{max}$ can be deduced which is given at the frequency of maximum dielectric loss ε″ for a certain temperature. Within experimental uncertainty, Eq. 1 described our data well. The term Δε describes the relaxational strength of the dipolar fluctuation under study.

Results

Differential scanning calorimetry

The DSC thermograms for selected samples are shown in Fig. 1 (see also Table 2). The samples are representative of the three backbone structures ODM, ETM and STM. Except for the ODM series and ETMH25 (not shown in Fig. 1) the samples show no endothermic peak at temperatures below T_g, indicated by arrows). The strong endothermic peaks below T_g for ETMH25 and ODMH25, and a very weak peak for ODM4F15 are due to the melting of the alkyl side chains [27, 28]. The ETM and STM series show decreasing T_g values with increasing length of side chain, which is attributed to the incorporation of longer perfluoroalkyl segments in the side chains. This behavior of decreasing T_g's in dependence of increasing fluorine content was also observed in other fluorinated side chain polymer systems [17]. Above T_g, the STM and ODM series show no additional endothermic peaks while longer side chains of the ETM series have additional peaks. The additional peak for ETM4F15 at around 436 K is assigned to order/disorder transition of the material in the bulk. This assignment is supported by temperature-dependent small-angle X-ray diffraction experiments (SAXS) and temperature-dependent ATR-IR [24]. Further work is in progress to explain the additional peaks between 390 K and 440 K for ETM4F19 and ETM6F19 (also see Table 2).

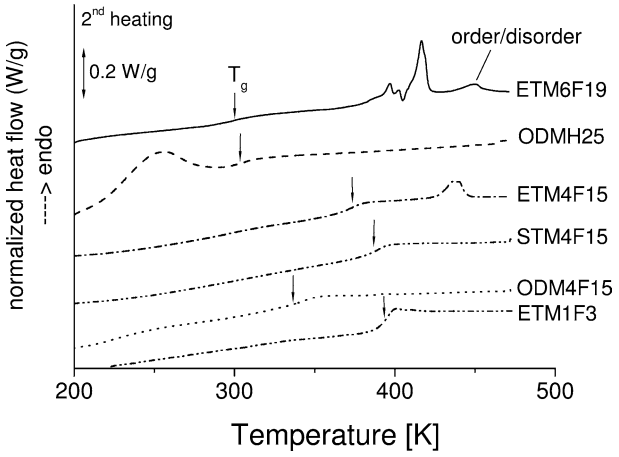

Fig. 1 Differential scanning calorimetry curves of samples ETM1F3, ETM4F15, STM4F15, ETM6F19, ODM4F15 and ODMH25 obtained from the second heating at a rate of 20 K/min. *Arrows* indicate the glass transition temperatures

These DSC results imply that for long fluorinated side chains, the fluorinated MI copolymers are able to form layered structures proven by the order/disorder transition for ETM4F15 and supported by the backbone–backbone distances (d values) as published in ref. [24]. However, the presence of the second side chain R^2 (alkyl chain or phenyl ring) possibly governs another organization of the fluorinated side chains in the bulk. The low enthalpy ($\Delta H_m = 1.9$ J/g, around 250 K) for alkyl side chain melting in ODM4F15 indicates that the presence of the hexadecyl chain R^2 results in a weak phase separation between the R_f-side chains and the hexadecyl side chains because of the alternating substitution pattern of the side chains and the helical-like state of the main chain [27, 28]. Nevertheless, as will be shown later in the paper, three main relaxation regions in ODM4F15 corresponding to the alkyl, backbone and fluoroalkane domains are observed from the dielectric spectra. The presence of the bulk phenyl ring governs a different material packaging in which the ordering of side chains is hampered. From the molecular dynamics perspective, motions related to the backbone will presumably not be hindered.

Dielectric spectroscopy

The compounds in Table 3 show dielectric spectra that look similar. At temperatures below 200 K, the spectra are characterized by one relaxation process with a

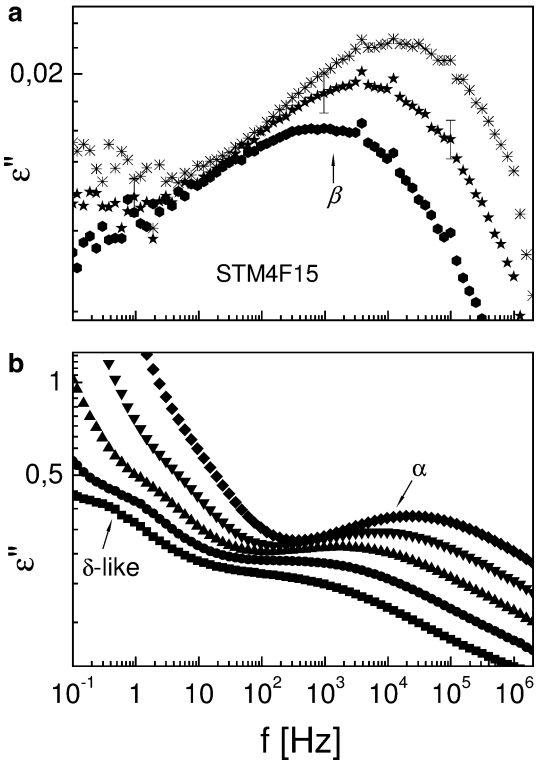

Fig. 2 **a** Compound STM4F15. Dielectric loss ε″ versus frequency at 160 K (*filled hexagon*), 170 K (*five point asterik*) and 180 K (*eight point asterik*) for the β process. **b** Two additional peaks α and δ-like are observed at different temperatures; (*filled square*) 320 K, (*filled circle*) 330 K, (*filled triangle*) 340 K, (*filled inverted triangle*) 350 K and (*filled diamond*) 360 K. The exponential increase in ε″ at low frequencies is caused by a conductivity contribution due to mobile charge carriers. For clarity, *error bars* are indicated on only one sample for the β process. Otherwise for the α- and δ-like processes, *error bars* are smaller than the size of the symbols

Table 3 Abbreviation of the alternating MI copolymers used in the study and their chemical structures

R^1	R^2		
	H	Phenyl	Hexadecyl
$-CH_2-CF_3$	ETM1F3	–	–
$-(CH_2)_4-NH-CO-C_7F_{15}$	ETM4F15	STM4F15	ODM4F15
$-(CH_2)_{11}CH_3$	ETMH25	STMH25	ODMH25
$-(CH_2)_4-NH-CO-C_9F_{19}$	ETM4F19	–	–
$-(CH_2)_6-NH-CO-C_9F_{19}$	ETM6F19	–	–

dielectric loss ε″ of less than 0.05. No conductivity contribution is observed within this temperature range. Above 200 K, the spectra can be described generally as composed of two or three relaxation processes and a conductivity contribution. In the following, the four relaxation processes will be referred to as β,α,δ-like and α_s according to the sequence of their mean relaxation times. Figure 2a shows the experimental results of the

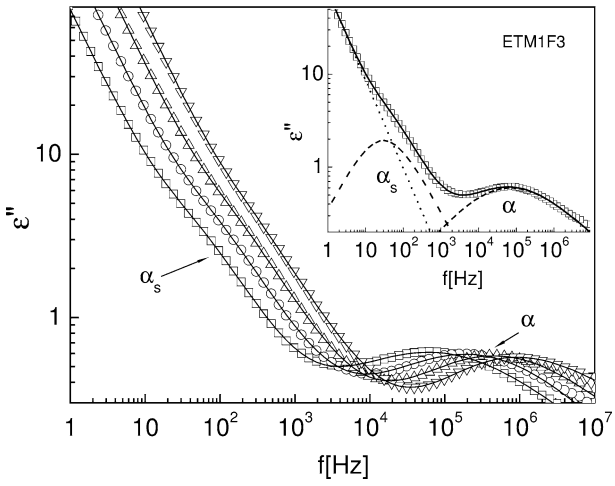

Fig. 3 Example of dielectric spectra for the copolymer ETM1F3 at different temperatures: (*open square*) 468 K, (*open circle*) 476 K, (*open triangle*) 484 K and (*open inverted triangle*) 492 K. The *inset* shows the separation of the two processes α and α_s with the HN fit function. The *dotted line* is the conductivity contribution and the continuous line is the superposition of the two *dashed curves*. The HN fit parameters are given in Table 4

dielectric loss ε″ as a function of frequency for compound STM4F15 at temperatures of 160, 170 and 180 K. One broad relaxation (β) peak is observed in this temperature range. In Fig. 2b, two more relaxations (α and δ-like) are observed in a broad temperature range with an additional conductivity contribution at low frequencies. At temperatures above the T_g, a further relaxation region (α_s-process) uniquely characterized by high relaxation strengths in sample ETM1F3 (Fig. 3) is detected.

To describe the experimental spectra quantitatively, the isothermal data of the dielectric losses ε″ were fitted according to Eq. 1. For instances where there are no conductivity contributions in the spectra, only the imaginary part of Eq. 1 was used to fit the peak and the conductivity parameters were ignored. Stable results from the fits were obtained for the relaxation times of the β-, α-, δ-like and α_s-processes of the respective copolymers. The accuracy in the determination of Havriliak–Negami (HN) fit-parameters (Table 4) was generally better than 10%. Figure 3 shows an example of the fitting results for the copolymer ETM1F3 at different temperatures, with the inset showing the separated processes and the conductivity contribution. It can be seen that the α- and α_s-processes are well separated from the conductivity. Figure 4 shows a representative activation plot of the relaxation processes for compounds ETM1F3, ETM4F15, ETM4F19 and ETM6F19. In this figure, the mean relaxation time (given at the frequency of maximum dielectric loss ε″ for a certain temperature) is plotted as $1/\tau_{max}$ in a logarithmic scale versus inverse temperature. Table 5 provides the fit parameters for all the compounds studied.

Table 4 Havriliak–Negami (HN) fit parameters for compound ETM1F3 shown in Fig. 3

Temperature (K)	σ_o ($\times 10^{-9}$)	a	HN fit parameters							
			α				α_s			
			$\Delta\varepsilon$	τ ($\times 10^{-7}$)	β	γ	$\Delta\varepsilon$	τ ($\times 10^{-3}$)	β	γ
468	3.9 ± 1.0	0.9 ± 0.1	3.1 ± 0.1	34 ± 0.2	0.5 ± 0.1	0.8 ± 0.1	5.5 ± 0.1	5.0 ± 0.2	0.8 ± 0.1	1.0 ± 0.1
476	8.3 ± 1.0	0.9 ± 0.1	2.8 ± 0.1	7.4 ± 0.2	0.5 ± 0.1	1.0 ± 0.1	5.5 ± 0.1	3.2 ± 0.2	0.8 ± 0.1	0.9 ± 0.1
484	16 ± 1.0	0.9 ± 0.1	2.7 ± 0.1	5.0 ± 0.2	0.6 ± 0.1	0.8 ± 0.1	5.1 ± 0.1	1.9 ± 0.2	0.9 ± 0.1	0.7 ± 0.1
492	31 ± 1.0	0.9 ± 0.1	2.8 ± 0.1	4.1 ± 0.2	0.6 ± 0.1	0.5 ± 0.1	4.6 ± 0.1	1.1 ± 0.2	0.9 ± 0.1	0.7 ± 0.1

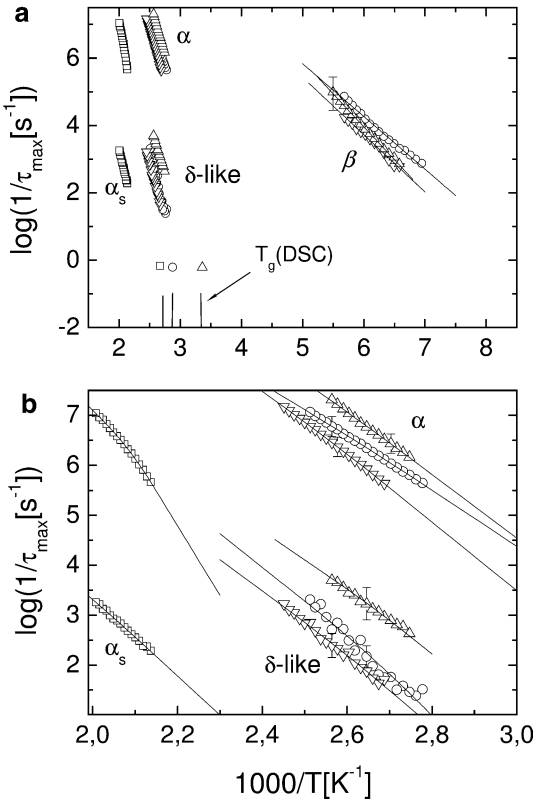

Fig. 4 **a** Activation plot of the β-, α-, δ-like and α_s-processes for the different compounds investigated. Calorimetric glass transition temperatures of ETM1F3 (*open square*), ETM4F15 (*open circle*) and ETM6F19 (*open triangle*) are indicated. No calorimetric T_g for ETM4F19 (*open inverted triangle*) was found. Arrhenius fits to the β-process according to Eq. 2 are also indicated. **b** An enlargement of the α, δ-like and α_s-processes showing the VFT fits (continuous lines) according to Eq. 4. The Arrheinius and VFT fit parameters are shown in Table 5. *Representative error bars* are indicated. Otherwise error bars are smaller than the size of the symbols, if not indicated otherwise

Discussion

The discussion of the results will be done in three steps. First, we present the effect of perfluoroalkyl side chains on the relaxation dynamics of the MI backbone. Secondly, by modifying the backbone structure using the second side group R^2 (with $R^2 \neq H$), we focus on the influence of R^2 on the dynamics of the side chain. Lastly, a comparison of the molecular relaxation will be made between unfluorinated side chain MI copolymers (ETMH25, STMH25 and ODMH25) and their fluorinated side chain counterparts (ETM4F15, STM4F15 and ODM4F15) of similar side chain lengths.

Perfluoroalkyl side chains

Figure 4 shows the temperature, T, dependence of the relaxation times of four samples that differ in the length of the side chain. The β-relaxation is observed in samples ETM4F15, ETM4F19 and ETM6F19. These three compounds have long side chains compared to ETM1F3 whose side chain is made up of only the CH_2–CF_3 group. The fact that the β-relaxation is observed in samples with long side chains and not in the short side chain polymer points out that the β-process originates from a defined minimum of side chain length. The temperature dependence of the relaxation times can be described by an Arrhenius equation,

$$\tau = \tau_o \exp\left[\frac{-E_a}{RT}\right] \tag{2}$$

with E_A denoting the activation energy ($\sim 35 \pm 5$ kJ/mol) and $\tau_o (= 1/2\pi\ \nu_o)$ a pre-exponential factor. τ is the relaxation time, R is the universal gas constant and T is the absolute temperature.

Fluoroalkane units are usually described as stiff rod-like segments with dipole moments parallel and perpendicular to the side chain axis [18]. The parallel component ($\mu_{\parallel}$) originates partly from the uncompensated end fluorine atom in the stiff alkyl parts of the perfluoroalkyl chain and partly from the net dipole moment of the succinimide ring of the MI copolymer backbone. The perpendicular component ($\mu_{\perp}$) comes as a result of contributions from the carbonyl and N–H groups, and a small fraction of the CF bonds (which amounts to about 16% of μ_{CF} due to the helical

Table 5 Vogel–Fulcher–Tammann (VFT) and Arrhenius fit parameters for all the compounds studied

	Arrhenius		VFT								
	β		α			δ-like			α_s		
	log ν_o (Hz)	E_a (kJ/mol)	Log ν_o (Hz)	A	T_o	log ν_o (Hz)	A	T_o	log ν_o (Hz)	A	T_o
ETM1F3	–	–	10.5	374 ± 37	391 ± 4	–	–	–	14.0	3,856 ± 51	139 ± 5
ETM4F15	12.9	30 ± 3	16.0[3]	2,481 ± 13	120 ± 1	11.0	1,028 ± 7	260 ± 10	–	–	–
ETM4F19	13.1	33 ± 2	16.4[3]	2,362 ± 261	153 ± 12	12.0	2,083 ± 58	172 ± 6	–	–	–
ETM6F19	14.9[3]	37 ± 3	18.0[3]	3,005 ± 35	117 ± 3	11.0	1,381 ± 5	200 ± 20	–	–	–
ETMH25	17.0[3]	34 ± 4[1]	–	–	–	12.7	1,005 ± 146	246 ± 10	–	–	–
STM4F15[2]	13.4	33 ± 2	15.0[3]	2,115 ± 30	142 ± 3	8.0 [c]	1,781 ± 83	83 ± 12	–	–	–
						9.5[d]	2,494 ± 803	65 ± 20			
STMH25	17.4[3]	35 ± 2	–	–	–	11.0	677 ± 6	302 ± 2	8.0	1,586 ± 118	174 ± 20
ODM4F15	16.0[3]	36 ± 4	17.5[3]	2,810 ± 20	104 ± 2	11.5	1,015 ± 13	240 ± 10	–	–	–
ODMH25	17.7[3]	37 ± 2	–	–	–	10.2	591 ± 32	272 ± 3	–	–	–

[1]Published in reference [27]
[2]Fit parameters indicated by continuous line, c, and dashed line, d, in Fig. 6b
[3]Values of log $\nu_o \geq 14$ are unphysical. Under these conditions, an extrapolation to the high temperature limit is not realistic. This is caused by few fitted data points

structure of the molecule [16]). The different dipole contributions are illustrated in Scheme 2.

A bimodal relaxation is expected as a result of the two net dipole contributions. However, the relaxation due to the $\mu_{\|}$ component is most unlikely to occur at low temperatures in this sort of a rod-like structure because it would involve large-scale motions. At high temperatures (probably around or above the T_g for polymers with long side chains), a relaxation through the $\mu_{\|}$ component would involve motion of the side groups along the molecular short axis. This may be considered analogous to the "δ-mode" in side-chain liquid crystalline polymers (SCLCP) [34]. At temperatures below T_g, the dual relaxation can be expected to occur simultaneously only for very short side chains owing to the proximity of the two net dipole contributions and a short side group able to make fast motions. An example of such duality was observed in compound ETM1F3 (Fig. 5). It was however not possible to separate the two processes and no reliable HN fit parameters were obtained. Therefore, it is not clear which relaxation process (I or II) corresponds to $\mu_{\|}$ and the other to $\mu_{\perp}$. From the intensity, location and the activation energy of the β-relaxation, we conclude that it should reflect a local motion of the side chain. The preceding dipole analysis affirms that this relaxation originates from the perpendicular component of the perfluoroalkane units. This assignment can be likened to the librational fluctuations of the mesogens in a potential formed by its neighbors in SCLCPs.

We now turn our discussion to the high temperature relaxations in Fig. 4. The relaxation of the MI backbone has been described by Tsuwi et al. [27] and coworkers recently. It is characterized by two dielectric relaxations: an in-plane fluctuation [28] of the succinimide ring and a

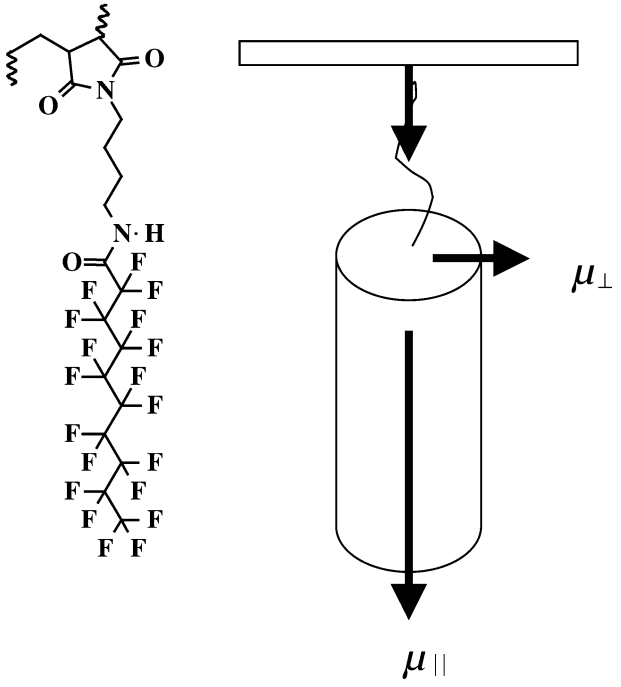

Scheme 2 Structure of the R_f side chain in ETM4F19 showing the perpendicular ($\mu_{\perp}$) and the parallel ($\mu_{\|}$) components of the dipole moment of the fluoroalkane unit

cooperative motion of at least two succinimide rings. The fluctuation of the succinimide ring was assigned to the dynamic glass transition process for all the copolymers studied in ref. [27]. We extend this argument to the fluorinated MI copolymers. Sample ETM1F3 has a T_g value of 392.2 K, which is the highest among the compounds indicated in Fig. 4. This value coincides well with the temperature obtained when the relaxation time

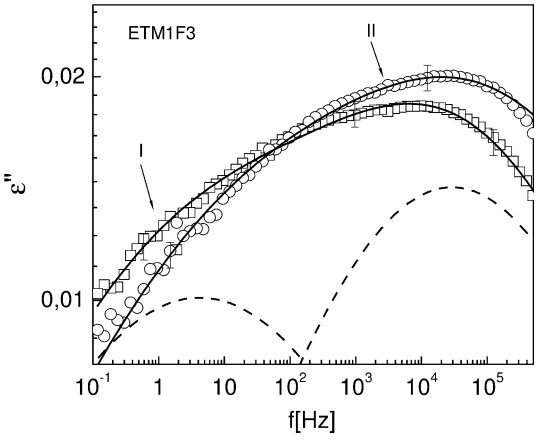

Fig. 5 Dielectric loss ε″ versus frequency for ETM1F3 at 204 K (*open square*) and 214 K (*open circle*). The data were fitted using Eq. 1 with the continuous line being the superposition of the two *dashed lines*. For clarity, processes I and II are indicated for the spectra at 214 K with the following HN fit parameters; process II:Δ ε = 0.1,τ = 0.007 s, $\beta = 0.23$ and $\gamma = 1$; process II:Δ ε = 0.15, $\tau = 1.5\times10^{-6}$ s, $\beta = 0.26$ and $\gamma = 1$. The parameters contain large uncertainties due to the difficulty in separating the two processes. The two relaxation processes originate from fluctuations of the two net dipole contributions ($\mu_{\|}$ and $\mu_{\perp}$) of the perfluorolkyl side chain

of the α-process is extrapolated to 100 s [35, 36], even though not true for all the copolymers studied. Nevertheless, we assign the α-process to the dynamic glass transition process of the copolymers in conformity with our earlier work [27]. The α-process is characterized by a Vogel–Fulcher–Tammann (VFT) [37–39] relaxation behavior described mathematically as

$$\tau_{\max} = \tau_o \exp\left[-\frac{A}{(T - T_o)}\right] \tag{3}$$

where $A = DT_o$ with D the fragility parameter and T_o is the Vogel temperature or the ideal glass transition temperature. The calorimetric T_g's of ETM4F15 and ETM6F19 are also indicated in Fig. 4. However, the values seem to be slightly higher than predicted by extrapolating the α-process to longer times [35, 36].

The molecular origin of the α-process in fluorinated MI copolymers can well be understood by considering the packaging of the polymer in the bulk based on structure analysis [24] and our previous [27] assignment. A subtle interplay between the dynamics of the polymer backbone and the attached side groups characterizes the α-relaxation. For shorter side chains, the α-process highly reflects backbone dynamics. For sample ETM1F3, it is therefore not surprising to observe this process occurring in temperature and frequency windows identical to that of the succinimide ring as reported in ref. [27]. The proximity of the CH_2–CF_3 group to the backbone results in a cooperative motion of the succinimide ring together with the side group hence the process occurs at elevated temperatures compared to the other samples. As for samples ETM4F15, ETM4F19 and ETM6F19 at least four CH_2 spacer groups are incorporated between the succinimide ring and the fluoroalkane groups allowing decoupling of backbone motions from side group motions. Unlike ETM1F3, the α-relaxation for ETM4F15, ETM4F19 and ETM6F19 occurs at lower temperatures because main chain motions are well decoupled from motions of the bulky perfluoroalkyl groups owing to their tendency to self-organize into rigid phases. The T_g's also show a clear tendency with respect to the spacer length dependence. Because ETM6F19 has longer spacer length than ETM4F15 and ETM4F19, its α-process is faster. Spacer-length dependence on the relaxation of the dynamic glass transition process in SCLCPs is well documented [40, 41], in which a similar argument can be extended to other side chain polymer systems. Longer spacers act as plasticizers thus lowering the T_g [40, 41]. The α-process is therefore considered, in this case, to be caused by motions of the main chain.

As suggested earlier in this paper, only the $\mu_{\|}$ component of the net dipole moment can be involved in large-scale motions of the side chains. However, it has to be assumed that for short spacers the perfluoroalkyl participate in cooperative motion of the main chain (e.g. ETM1F3). For longer side chains, the phase separated perfluoroalkyl perform a δ-like relaxation as observed for samples ETM4F15, ETM4F19 and ETM6F19. In order to verify the magnitude of the dipole contribution for the δ-like relaxation, theoretical calculations of dipole moment μ were carried out for perfluoroalkyl segments, including the CF_2–CF_3 segment, and succinimide unit [27] using GAMESS [30, 31]. A value of $\mu = 3.0 \pm 0.5\times10^{-30}$ As m for the CF_2–CF_3 group was obtained. From fits of dielectric spectra according to Eq. 1, the dipole contribution to the relaxation process was estimated using the relation [42–44] (neglecting the Kirkwood–Fröhlich correlation factor)

$$\Delta\varepsilon \approx n\frac{\mu^2}{3k_B T\varepsilon_o}. \tag{4}$$

In this notation,μ is the net dipole moment involved in the relaxation, n is the dipole density, k_B is the Boltzmann constant, T is the temperature and ε_o as explained in Eq. 1. The estimate gives a dipole contribution in the range $2.2–4.0\times10^{-30}$ As m within an uncertainity of ±20% for the different compounds. We conclude that the molecular origin of the δ-like relaxation in fluorinated MI copolymers is a relaxation of the perfluoroalkyl domain of the side chains.

Above T_g, the α_s-process is observed. This has been assigned [27] to a cooperative relaxation of at least two succinimide rings. The α_s-relaxation is observed in sample ETM1F3 and not in the other three samples in

Fig. 4. This can be understood given that only a CH_2–CF_3 group forms the side chain of this sample, and therefore backbone dynamics dominate. For long perfluorinated side chains, which to a greater extent influence the orientation of the backbone, the α_s-relaxation is not observed. One possible explanation is that the long and stiff perfluoroalkyl segments govern a backbone conformation that does not favor a relaxation through the α_s mode. This means that large-scale backbone mobility is hindered, as also was found to be the case with longer aliphatic side chains [27]. (The α_s-process was not detected for samples ETM4F15, ETM4F19 and ETM6F19).

Influence of R^2 on backbone dynamics

In order to discuss the relaxation dynamics of the different MI copolymer backbones (ETM, STM and ODM), we select samples with identical composition at R^1. Samples ETM4F15, STM4F15 and ODM4F15 have each 4 CH_2 spacer units and 15 F atoms on the side chains. The molecular dynamics of the ETM4F15 backbone has been discussed earlier in this paper. We now compare the temperature-dependence of the relaxation times for the three samples (Fig. 6a).

Except for ODM4F15, the two other samples do not show a pronounced effect on the β-relaxation. The slight high temperature-shift of the β-process by the introduction of a phenyl ring on the backbone may be due to a different side chain packaging introduced by the phenyl group, thus permitting slower motions. The slight shift was also observed for MI compounds with purely alkyl side chains (to be shown later in Fig. 8). The compound ODM4F15 has a faster β-process than the other two samples. The sample's backbone is modified by including a hexadecyl side chain on R^2. The location and nature of the activation, reflects motion similar to that reported [27] in poly(ethene-*alt*-*N*-alkylmaleimide) copolymers in which the CH_2–CH_3 was assigned to the β-relaxation. The β-relaxation of the ODM4F15 sample is therefore assigned to fluctuations of the terminal end groups of the hexadecyl side chain and not the perfluoroalkyl segment end groups.

The three main chain structures do not have a significant influence on the fluctuation of the succinimide ring (α-process). The slight shift of the ODM backbone to faster times for the α-process can be explained in terms of the plasticization effect of the hexadecyl side chain. A similar behavior is observed for the δ-like process. A discontinuity of the δ-like process due to the STM backbone is noticeable (Fig. 6b). Comparable to the "δ-process" in SCLCPs, such discontinuities are associated with a phase transition [45, 46] or a molecular rearrangement. The product $T\Delta\varepsilon$ (which would be constant for an ideal Debye relaxation) (Fig. 7) reflects the

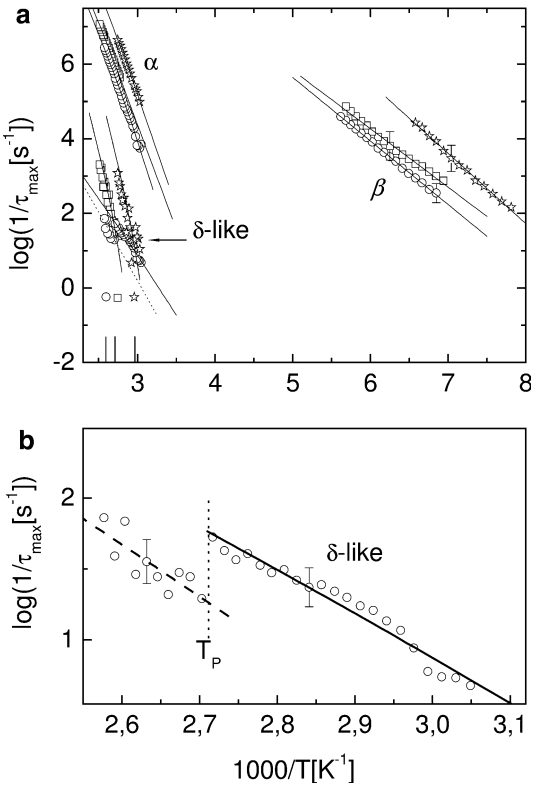

Fig. 6 **a** Activation plot showing β, α and δ-like processes for compounds with varied backbones: (*open square*) ETM4F15, (*open circle*) STM4F15 and (*asterisk*) ODM4F15. The lines are VFT fits with the fit parameters indicated in Table 5. **b** A discontinuity in the δ-like process for sample STM4F15, which may probably be a result of a phase transition or a change in the dynamics at temperature T_P (*dotted line*)

microstructure of the different systems. For ETM4F15, temperature dependence is not observed with respect to the α- and the δ-like relaxations both above and below T_g. For ODM4F15 similar dependences are also found. In contrast, STM4F15 shows an increase in $T\Delta\varepsilon$ for both the α- and the δ like relaxations but especially the δ like fluctuations. This is explained by the increase in mobility at higher temperatures.

Dynamics in unfluorinated (R_h) and fluorinated (R_f) side chain MI copolymers: a comparison

Figure 8 is an activation plot showing temperature dependence of the relaxation times for both the unfluorinated and fluorinated side chain MI copolymers. The two types of side chains (R_h and R_f) show profound differences in their relaxation rates of the β-process. Alkyl side chains have faster β-process (denoted as β_h) than the fluoroalkyl counterparts (β_f). This can be understood given that the molecular origins of the relaxations differ. Both have been assigned to librational

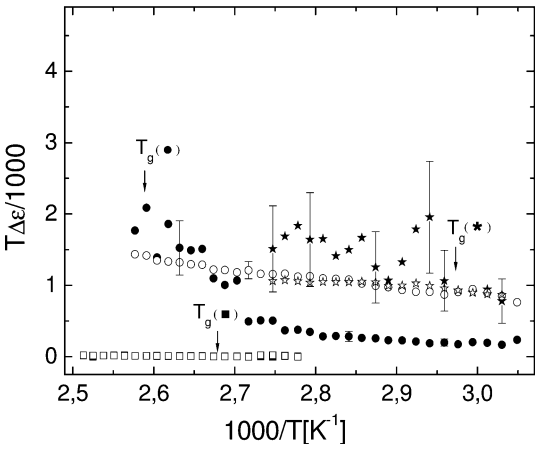

Fig. 7 Product $T\Delta\varepsilon$ for the α (*open symbols*) and δ-like (*closed symbols*) processes for samples ETM4F15 (*open square*, *filled square*), STM4F15 (*open circle*, *filled circle*) and ODM4F15 (*open asterisk*, *filled asterisk*). Calorimetric T_gs are indicated by *arrows*. A gentle increase in $T\Delta\varepsilon^{(\alpha)}$ and a sudden increase in $T\Delta\varepsilon^{(\delta\text{-like})}$ towards T_g for STM4F15 with temperature are shown. For clarity, *error bars* are indicated only on two samples for the δ-like process

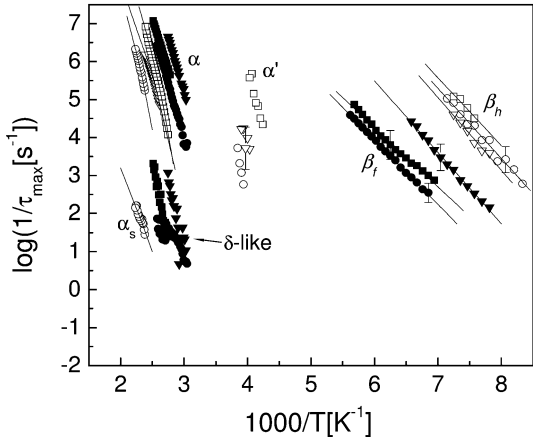

Fig. 8 Activation plot showing β,α′,α, δ-like and α $_s$-relaxations for R_h (*open symbols*) and R_f (*closed symbols*) side chain MI copolymers. The compounds are: ETMH25 (*open square*), ETM4F15 (*filled square*), STMH25 (*open circle*), STM4F15 (*filled circle*), ODMH25 (*open inverted triangle*) and ODM4F15 (*filled inverted triangle*). The β-process has been labeled *h* and *f* to differentiate it from the unfluorinated and the fluorinated copolymers respectively. The α′-process represents glassy dynamics of the alkyl side chain. *Representative error bars* are indicated for the β- and α′-processes

motion at the terminal position of the side chain. Alkyl side chains have an additional relaxation (α′-process) below T_g, which has been attributed to glassy dynamics of the alkyl side chain [27]. Unlike the β-process, the relaxation rates of the MI copolymer backbone (α-process, which is basically motion of the succinimide ring) show an opposite trend. The main chains attached with fluorinated side chains show faster dynamics than the alkyl ones. This can be explained as follows [47, 48]: due to microphase separation between the fluoroalkyl segments and the copolymer backbone, a reduced concentration of stiff moieties in the neighborhood of main chain segments results in an increased backbone mobility thus shifting relaxations to shorter times. When viewed from another perspective, the slow α-relaxation of the R_h-side chain attached backbone may be due to a higher packaging density of the alkyl chains around the backbone thus reducing its mobility. In this regard, R_h MI copolymers would then have an increased packaging density compared to the phase separated R_f copolymers. The change of the relaxation of the main chain (α-process) to shorter times may just be an indication of phase separation in side chain polymer systems. As observed from wide and small angle X-ray diffraction experiments [24], all polymers investigated except ETM1F3 show layered structure at room temperature [24] proving that they are indeed phase separated. Only ODM4F15 has no defined layered structure, but shows phase-separated domains as well.

The dynamic glass transition process in both R_h and R_f MI copolymers reflects the motion of the main chain [27] (succinimide ring), however the scaling of the α-process with calorimetric T_g's in R_f MI copolymers does not seem to hold in all cases. In fact, the T_g's as obtained from DSC are closer to the δ like process than the α-relaxation. This could indicate that the DSC detected more of R_f domain relaxations than the backbone glass transition motion. The α_s-relaxation, which is a cooperative motion of at least two succinimide rings [27], is observed strongly in the STMH25 sample and not in the other two R_h series. It was not possible to observe the α_s-process beyond three methylene groups on the side chain of ETM backbone as demonstrated in ref. [27]. The observation of the α_s-process in STMH25 compound indicates further just how influential the phenyl ring is on the dynamics of the main chain. Because of the bulky nature of the phenyl ring, increased free volume favors the cooperative motion of the succinimide rings leading to relaxation through the α_s-mode. For the R_f series of compounds, except ETM1F3, the α_s-relaxation may have been suppressed by the α-relaxation.

Conclusion

The molecular dynamics of MI copolymers with fluorinated side chains have been studied by broadband dielectric spectroscopy. Differential scanning calorimetry was used to determine thermal transitions of the copolymers, which were found to exhibit no melting of the fluoroalkyl side chains below the glass transition temperature. Due to the microphase separated structure of the polymer systems, the dynamics is mainly

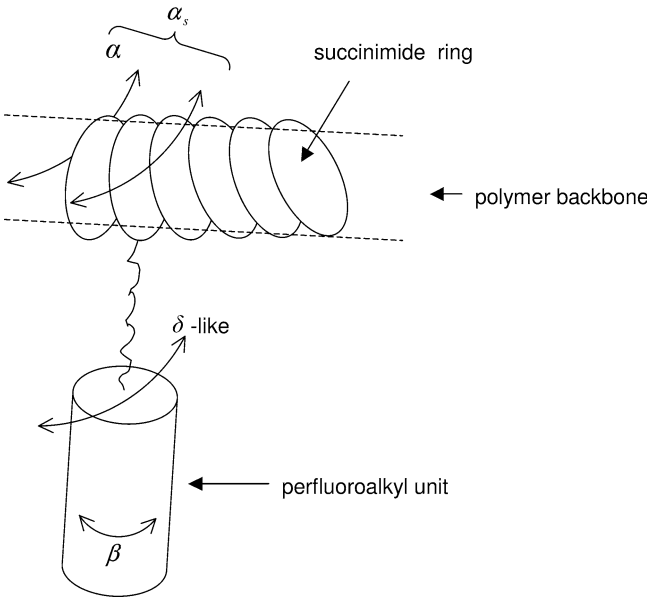

Scheme 3 Illustration of the different relaxation mechanisms exhibited by the MI copolymers. The α- and α_s-relaxations originate from backbone motions, while the β- and the δ-like processes are due to side chain relaxations

characterized by independent relaxations in the different domains. The fluoroalkyl side chains exhibit a bimodal relaxation due to the perpendicular and parallel components of the dipole moment of the fluorocarbon segment, however this is only noticeable for short side chains. The dynamic glass transition process, which reflects motion of the main chain, is shifted to lower temperatures by substituting the alkyl side chains with fluoroalkyl ones. It can be concluded that the T_gs obtained by DSC for the fluorinated MI copolymers are higher than those obtained in dielectric spectroscopy, probably because of the R_f groups. The presence of a second side chain R^2 governs the dynamics of the fluorinated MI copolymers due to a different packaging of the backbone. When compared with unfluorinated copolymers, the fluorinated MI copolymers exhibit a dynamics similar to microphase separated polymer systems, while the unfluorinated MI counterparts, on the other hand, do not. The unfluorinated copolymers are therefore perceived to be more densely packed than the R_f coplymers. Finally, the proposed molecular dynamics of fluorinated MI copolymers is illustrated schematically in Scheme 3.

Acknowledgements Financial support for J. Tsuwi by the German academic exchange service (DAAD) is acknowledged. D. Appelhans and R.-C. Zhuang acknowledge the German Ministry of Research and Education (BMBF) for financial support. The authors also thank Mrs. Lehmann for carrying out the synthesis of MI copolymers and Dr. H. Komber for the NMR experiments.

References

1. Castner DG, Grainger DW (eds) (2001) Fluorinated surfaces, coatings, and films, ACS symposium series, vol 787. American Chemical Society publication, Washington
2. Hougham G, Cassidy PE, Johns K, Davidson T (eds) (1999) Fluoropolymers . Kluwer/Plenum, New York
3. Corpart JM, Dessaint A (1997) Melliand E135:78
4. Corpart JM, Dessaint A, Collete C (eds) (1994) Fluorine in coatings. In: 2nd International conference; Paint Research Association, Teddington
5. Bierbrauer CJ, Goebel KD, Landucci DP (1979) Amer Dyestuff Rep 68(6):19
6. Song K, Twieg JR, Rabolt JF (1990) Macromolecules 23:3712
7. Gottwald A, Pospiech D, Jehnichen D, Häußler L, Friedel P, Pionteck J, Stamm M, Floudas G (2002) Macromol Chem Phys 203(5–6):854
8. Viney C, Twieg RJ, Russell TP (1990) Mol Liq Cryst 182B:291
9. Pittman AG (1972) In: Wall LA (ed) Fluoropolymers, vol 25. Wiley, New York, p 419
10. Höpken J, Möller M (1992) Macromolecules 25:1463
11. Davidson T, Griffin AC, Wilson LM, Windle AH (1995) Macromolecules 28:354
12. Wilson LM, Griffin AC (1994) Macromolecules 27:1928
13. Höpken J, Möller M (1992) Macromolecules 25:2482
14. Lorenz K, Frey H, Stühn B, Mülhaupt R (1997) Macromolecules 30:6860
15. Stark B, Stühn B (1998) Macromolecules 31:5415
16. Trahasch B, Stühn B, Lorenz K, Frey H (1999) Macromolecules 32:1962
17. Pospiech D, Häussler L, Jehnichen D, Kollig W, Eckstein K, Grundke K (2003) Macromol Symp 198(1):421
18. Floudas G, Antonietti M, Förster SJ (2000) Chem Phys 113(8):3447
19. Hendlinger P, Laschewsky A, Bertrand P, Delcorte A, Legras R, Nysten B, Möbius D (1997) Langmuir 13(2):310
20. Corpart JM, Girault S, Juhue D (2001) Langmuir 17(23):7237
21. van Ravenstein L, Ming W, van de Grampel RD, van der Linde R, de With G, Loontjes T, Thüne PC, Niemantsverdriet JW (2004) Macromolecules 37:408
22. Pospiech D, Häußler L, Eckstein K, Komber H, Voigt D, Jehnichen D, Friedel P, Gottwald A, Kollig W, Kricheldorf HR (2001) High Perform Polym 13:275
23. Grundke K, Pospiech D, Kollig W, Simon F, Janke A (2001) Colloid Polym Sci 279(8):727
24. Appelhans D, Wang ZG, Zschoche S, Zhuang RC, Häussler L, Friedel P, Simon F, Jehnichen D, Komber H, Grundke K, Eichhorn KJ (in Press) Macromolecules
25. Kwok DY, Li A, Lam CNC, Wu R, Zschoche S, Pöschel K, Gietzelt T, Grundke K, Jacobsch HJ, Neumann AW (1999) Macromol Chem Phys 200:1121
26. del Rio OI, Kwok DY, Wu R, Alvarez JM, Neumann AW (1998) Colloid Surf A Physiochem Eng Aspects 143:197

27. Tsuwi J, Appelhans D, Zschoche S, Friedel P, Kremer F (2004) Macromolecules 37(16):6050
28. Block H, Grooves R, Walker SM (1972) Polymer 13:527
29. Bauer B et al (1998) SuSE Linux 8.2, Manual. ISBN 3-930-419-67-X
30. Schmidt MW, Baldridge KK, Boatz JA, Elbert ST, Gordon MS, Jensen JH, Koseki S, Matsunaga N, Nguyen KA, Su S, Windus TL, Dupuis M, Montgomery JA (1993) J Comput Chem 14:1347
31. Friedel P (1998–2003) RESMAIN, Program for building linear and hyperbranched polymers with optional parameters choosing constitutional and conformational statistics. Institute of Polymer Research, Dresden
32. Kremer F, Schönhals A (2003) In: Kremer F, Schönhals A (eds) Broadband dielectric spectroscopy, Chap 2. Springer, Berlin Heidelberg New York
33. Havriliak S, Negami S (1966) J Polym Sci C 14:99
34. Kremer F, Schönhals A (2003) In: Kremer F, Schönhals A (eds) Broadband dielectric spectroscopy, Chap 10. Springer, Berlin Heidelberg New York
35. Donth E (1981) Glassübergang. Academie-Verlag, Berlin
36. Angell CA (1995) Science 267:1924
37. Vogel H (1921) Phys Z 22:645
38. Fulcher GS (1925) J Am Chem Soc 8:339
39. Tammann G, Hesse G (1926) Anorg Allg Chem 156:245
40. Schönhals A, Carius HE (2000) Int J Polym Mater 45:239
41. Kremer F, Schönhals A (2003) In: Kremer F, Schönhals A (eds) Broadband dielectric spectroscopy. Springer, Berlin Heidelberg New York, pp 400–406
42. Kirkwood JG (1939) J Chem Phys Soc 7:911
43. Böttcher CJF (1973) Theory of Electric Polarization, vol 1, 2nd edn. Elsevier, Amsterdam, p 181
44. Fröhlich H (1958) Theory of dielectrics. Oxford University Press, London
45. Kremer F, Schönhals A (2003) In: Kremer F, Schönhals A (eds) Broadband dielectric spectroscopy. Springer, Berlin Heidelberg New York, pp 397–409
46. Schick C, Sukhorukov D, Schönhals A (2001) Macromol Chem Phys 202:1398
47. SchönhalsA, Geßner U, Rübner J (1996) Macromol Chem Phys 196:1671
48. Lipatov SY, Tsukruk VV, Shilov VV (1983) Polym Commun 24:75